Modeling of Soil Water Distribution in a Small Mid-Latitude Watershed on the British Isle for Short Term Landslide and Flood Risk Assessment

Karam, H. A., Blackett, M., da Silva, R. B. P., Rojas, J. L. F., Filho, A. J. P., Peña, C. A. S., Panduro, I. L. V., Siqueira, B. S. & Suazo, J. M. A

DOI 10.11137/1982-3908_2024_47_57297
ISSN 0101-9759
ESSN 1982-3908

Publisher: Anuário do Instituto de Geociências

Anuário do Instituto de Geociências
Universidade Federal do Rio de Janeiro
https://revistas.ufrj.br/index.php/aigeo/

ISSN 0101-9759
e-ISSN 1982-3908

Modeling of Soil Water Distribution in a Small Mid-Latitude Watershed on the British Isle for Short Term Landslide and Flood Risk Assessment

Modelagem da Distribuição de Água no Solo de Uma Pequena Bacia Hidrográfica de Latitude Média na Ilha Britânica para Avaliação de Riscos de Deslizamento e Inundação em Curto Prazo

Hugo Abi Karam[1], Matthew Alexander Blackett[2], Raphaella Barros Pereira da Silva[1], Jose Luis Flores Rojas[3], Augusto José Pereira Filho[4], Cesar Arturo Sanchez Peña[5], Isela Leonor Vásquez Panduro[6], Brenda Santos Siqueira[7] & Julio Miguel Angeles Suazo[8,9]

[1]Universidade Federal do Rio de Janeiro, Centro de Ciências Matemáticas e da Natureza, Instituto de Geociências, Departamento de Meteorologia, Rio de Janeiro, RJ, Brasil
[2]Coventry University, EEC School of Energy, Construction and Environment, Coventry, Inglaterra, Reino Unido
[3]Instituto Geofísico do Peru, Lima, Peru
[4]Universidade de São Paulo, Instituto de Astronomia, Geofísica e Ciências Atmosféricas, Departamento de Ciências Atmosféricas, São Paulo, SP, Brasil
[5]Instituto Nacional de Pesquisas Espaciais, São José dos Campos, SP, Brasil
[6]Instituto Nacional de Pesquisas Espaciais, Centro de Previsão do Tempo e Estudos Climáticos, São José dos Campos, SP, Brasil
[7]Universidade Federal do Rio de Janeiro, Programa de Pós-Graduação em Engenharia Civil, Rio de Janeiro, RJ, Brasil
[8]Universidad Nacional Autónoma de Tayacaja Daniel Hernández Morillo, Facultad de Ingeniería Forestal y Ambiental, Pampas, Perú
[9]Universidad Tecnológica del Perú, Faculdad de Ingeniería Industrial, Lima, Perú

E-mails: hugo@igeo.ufrj.br; m.blackett@coventry.ac.uk; barross.raphaella@gmail.com; jflores@igp.gob.pe; augusto.pereira@iag.usp.br; arturo66cta@gmail.com; iselavp@gmail.com; brenda_santos87@yahoo.com.br; julio_as_1@hotmail.com
Corresponding author: Hugo Abi Karam; hugo@igeo.ufrj.br

Abstract

The R-TopModel hydrological model coupled with two landslide and flood probability distribution models was applied to simulate the daily hydrological conditions of a small catchment in the Midlands of the British Isles, throughout 2017. Originally, the methodology was applied to a risk area in the tropical region. In this work, the application was extended to mid-latitude watersheds. The hydrographic basin around the Carsington Water dam (located in the Midlands of the Great Britain) is chosen because it presents risks. The model Nash-Sutcliffe Efficiency for the upstream discharge from the Carsington Water dam reached 50% with a correlation coefficient of the order of 70%, an acceptable value considering the seasonal effects of the dam on evapotranspiration and higher soil permeability. Modeling the distribution of soil moisture and excess surface water allowed obtaining the spatial distribution of the maximum conditional probability of landslides and floods in the Carsington Water catchment. These probability maps obtained are consistent with long-term susceptibility maps for Great Britain.

Keywords: R-TopModel; Hydrometeorological hazards; Carsington Water-UK

Received: 06 March 2023; Accepted: 10 September 2023

Resumo

O modelo hidrológico R-TopModel acoplado a dois modelos de distribuição de probabilidade de deslizamento e enchente foi aplicado para simular as condições hidrológicas diárias de uma pequena bacia hidrográfica das terras médias das Ilhas Britânicas, ao longo de 2017. Originalmente, a metodologia foi empregada a uma área de risco de região tropical. Neste trabalho, a aplicação foi estendida para bacias hidrográficas de latitudes médias. Escolheu-se a bacia hidrográfica da represa Carsington Water, localizada no Centro-Norte das Inglaterra, por apresentar riscos. A efficiência de Nash-Suftcliffe do modelo para a vazão emergente da represa de Carsington Water alcançou 50% com uma coeficiente de correlação de aproximadamente 70%, valores aceitáveis considerados os efeitos sazonais da evapotranspiração e a permeabilidade do solo. A modelagem da distribuição da umidade do solo e do excesso da água a superfície permitiu obter a distribuição da máxima probabilidade de deslizamentos e enchentes ao redor de Carsington Water. Os mapas obtidos são consistentes com mapas de suscetibilidade de longo prazo da Grã-Bretanha.

Palavras-chave: R-TopModel; Perigos hidrometeorológicos; Hidrologia de Carsington Water-UK

1 Introduction

Hydrologically caused natural hazard events are becoming increasingly common in an era of climate change. Such natural hazard events include cyclones (inside and outside the tropics), floods, and rainfall-induced mass movement events. With respect to the latter, Froude and Petley (2018) showed an overall increasing trend in the number of mass movement events between 2004 and 2016 and a correspondingly high correlation (0.81) between average daily precipitation and average daily landslides, every month for the same period in South America. Their results support the hypothesis that the correlation is valid for any mountainous terrain. However, we can only assume that this correlation will be higher in topographically more extreme regions and/or regions with deep and unstable soils. It is more necessary than ever for scientists to better understand and model these events so that a reliable short-term forecast and associated mitigation measures can be applied. There are two main causes of rain-induced mass movements: 1) the presence of surface water (excess precipitation minus infiltration), which can cause significant erosion on a sloped surface, and 2) the presence of water within the slope that adds weight to the slope, provides a means of lubrication, and creates a positive pore water pressure.

One model that has been widely used for several decades to simulate rainfall runoff (and, correspondingly, rainfall infiltration into the soil) resulting in the distribution of rainfall in soil is the TopModel (Beven & Kirkby 1979). This model can be parameterized with regionally specific soil, topography and rainfall characteristics to predict how the surface will react to rainfall events and the possibility of water-induced landslides (Devia, Ganasri & Dwarakish 2015). In this last aspect, of modeling the probability of landslides, the hydrological model (e.g., TopModel) needs to be coupled to a soil mass movement model (e.g., a physical linear landslide model).

The TopModel was originally developed for mid-latitude regions where rainfall events can be assumed to be homogeneous over the surface of the watershed, that is, the prevalence of stratiform precipitation is assumed (Beven & Kirkby 1979). Since its development, however, it has also been widely applied in the tropics, for example in Venezuela (Gomez & Kavzoglu 2005) and Guatemala (Preti & Letterio 2015) and in the State of Rio de Janeiro, where extreme convective events present heterogeneous precipitation (Karam 2014). Next, the improved hydrological TopModel for convective heterogeneous rainfall was applied to simulated landslides and a risk index associated with dangerousness and contingent probability, focusing on the Metropolitan Region of Rio de Janeiro. The results were presented in two master's dissertations accomplished in the Post-Graduation Program Meteorology at the Geo-sciences Institute of the Federal University of Rio de Janeiro (Siqueira 2017; Peña 2018).

In recent times, the application of the TopModel has been limited in temperate regions, such as northern Europe and in particular the British Isles, where precipitation causes and patterns are considerably different from the tropics, but where induced mass movements by rain are equally prevalent. This is unfortunate, as one of the key features of the British Isles, and the UK in particular, is its dense network of rain gauges (3285 meters or 1 per 74 km^2) (Burt 2010) that can provide empirically recorded data for input into TopModel.

Since 2015, the dense network of rain gauges in the UK has been supplemented with a 1km resolution daily and monthly rainfall estimation system: CEH-GEAR (available at: https://eip.ceh.ac.uk/rainfall) (Keller et al. 2015). In this system, gridded precipitation values are estimated by interpolation of rainfall observed from all UK rain gauges (Keller et al. 2015). Unusually too, the UK has a very varied topography for a relatively small country (242000 km^2), with flat plains to the south and east and mountains reaching over 1000 m in Wales and Scotland.

Given these characteristics and the existence of high-resolution rainfall data (both actual and modeled), the reliability of applying TopModel to this UK dataset is currently excellent, although it also offers the potential to gain more information on 1) how improve TopModel for application in similar environments and 2) how to improve the prediction of landslides induced by rainwater in landslide-prone regions of the country. Figure 1 shows the topography and the landslide potential for Great Britain.

1.1 Objectives

In this work, the R-TopModel hydrological model is applied to simulate the surface water distribution in the area of the Carsington Water dam, in the Midlands of England. Furthermore, the hydrological model is coupled with a surface landslide model and a parametric flood surface model to assess both potential landslide and flood indices.

The associated goals are: 1) to obtain a better understanding of the specific location parameters of the hydrological modeling (R-TopModel) when coupled with the landslide proxy risk model proposed by Karam (2014); 2) to amend the system that was first applied also to topography of the State of Rio de Janeiro in Brazil by Siqueira (2017) and Peña (2018), to the topographic features in the British Isles; 3) to apply the coupled system to British Isles precipitation and river flow data (both measured data and high spatial resolution topography data of 50 m); and 4) to evaluate the model performance in retrospective prediction of water-induced landslides and flow in high resolution in small catchments of the British Isles and in its application to mid-latitude regions generally.

A careful evaluation of the parameters of the coupled models is necessary for a risk assessment system. The present work seeks to determine efficient parameters of the hydrological model, so that the numerical realization of the distribution of water in the soil and surface can be applied to assess the risk of floods and landslides. Customization of the system to resolutions of the order of 100 m and application of the model to risk prone areas of the British Isles depend on the correct evaluation of the parameters.

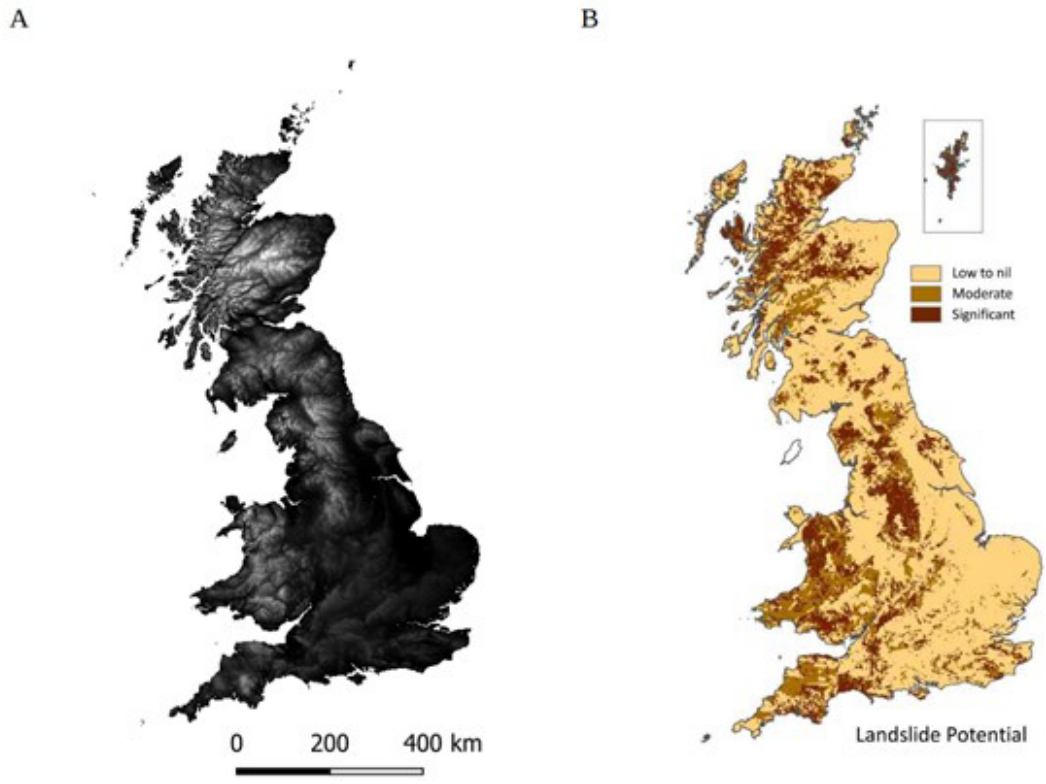

Figure 1 A. Topography of Great Britain (Danielson & Gesch 2011); **B.** Landslide potential in Great Britain (National Landslide Database 2023).

2 Methodology

In this section, we present the data source and methods used to obtain soil water saturation deficit, landslide and flood risk distributions.

2.1 Watershed Topography

The topography of the area of interest was available in the digital elevation model OS Terrain 50 (Ordnance Survey 2017) (Figure 1A). The landslide potential distribution on the British Isle is shown in Figure 1B. The Carsington Water catchment is located in the English Midlands, where there is significant potential risk, with hills west and northward and aquifers eastward.

2.2 Carsington Water Watershed

The Henmore Brook receives the Carsington outflow (Figure 2), being itself only a small catchment that is part of the complex Trent river regional basin in the Midlands.

The Henmore brook (identified in the UK reference grid by SK 242501, Station 28103) shows a catchment area of 15.8 km^2 (Marsh & Hannaford 2008). Some open-sky mines of limestone are present in the hills at northward Carsington Water. These mines can contribute to the inferior quality of brook water, where mercury and its compounds, and Poly-brominated diphenyl ether (PBDE), were discovered, both priority hazardous substances (ED-UK 2023). Henmore Brook Station 28103 use a rectangular thin-plate weir for measuring outflows from Carsington Water. Following the brook southward, a second station is found along Henmore Brook at Ashbourne (reference Station 28058). In that, it is used a crump profile flat V weir, 6.0 m wide, within vertical wing walls, built up into a low flood bank with no arrangements to deal with non-modular discharge. The catchment shows moderate relief, draining drift-free Millstone Grit and Carboniferous Limestone. The catchment is responsive and the land use is composed predominantly of forest and pasture, and some moorland (Marsh & Hannaford 2008).

2.3 Precipitation Data

In this work, daily data of precipitation and flow measured in 2017 in the Carsington Water dam area were used. The data source is the UK National River Flow Archive, Environment Agency-UK (2023). The database is available from 1-Jan-1961 to 31-Dec-2017. The precipitation and discharge data series are shown in Figure 3.

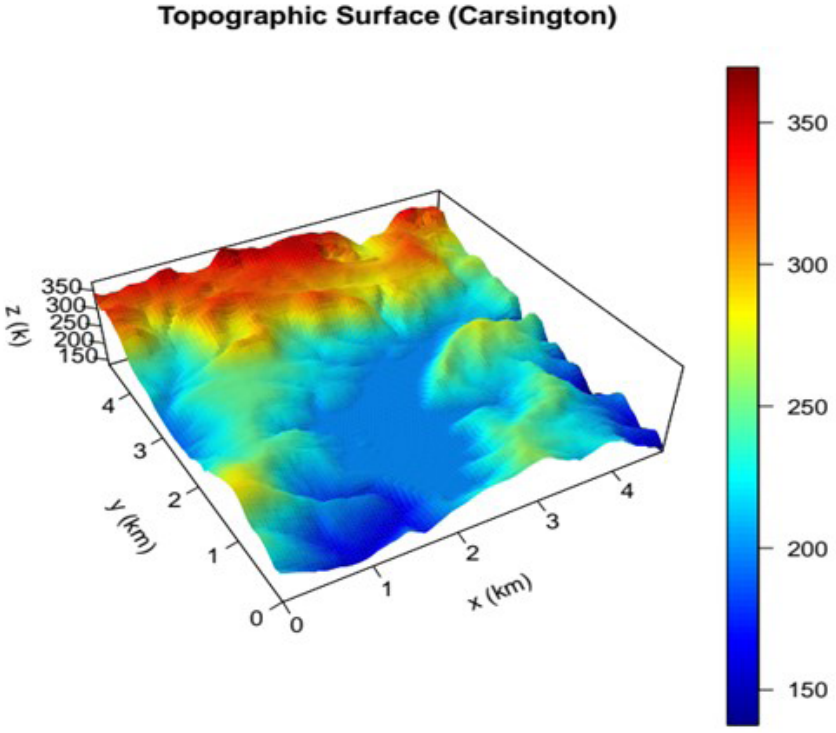

Figure 2 Perspective of Carsington Water dam and its small watershed in the center-east of Great Britain-UK. The Carsington Water dam is located in the central position of the map (53.0587436°N, -1.63258027°W).

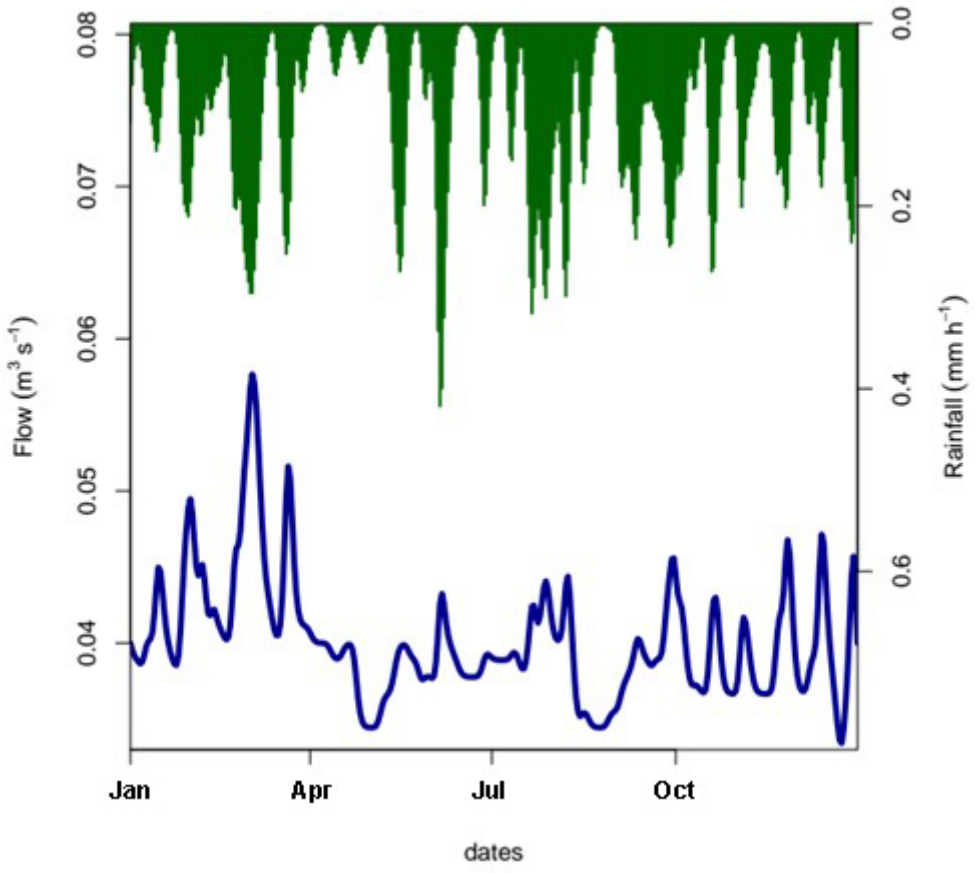

Figure 3 Daily data series of precipitation (mm h^{-1}) [impulses] and current flow (m^3 s^{-1}) [solid line] in 2017 at the outlet of Carsington Water Dam in the Midlands of England.

2.4 Flow Data

The flow data comes from the monitoring station called Carsington Outflow (id. number 8103, grid ref. SK242501) at Henmore Brook entry, during a year period (2017). Data are available for the period since 1998. The average flow rate is small, 0.05 m^3s^{-1}, of which the base flow corresponds to 88%. The quantile distribution shows the values 0.03 m^3s^{-1} (Q95%), 0.04 m^3s^{-1} (Q70%), 0.05 m^3s^{-1} (Q50%), and 0.1 m^3s^{-1} (Q10%). These flows are associated with an annual mean precipitation of 1028 mm, a mean annual runoff of 97 mm and a mean annual loss of 931 mm. A few kilometers downstream at the Station Henmore Brook 28058, in Ashbourne, SK176463, the flow has already been increased by the concentrated flow from the adjacent responsible surfaces. Gaussian convolution was applied to slightly reduce the unsystematic observational errors present in the original series.

2.5 The Hydrological Distributor TopModel

Beven, Kirkby and Freer (2021) published a comprehensive review of the TopModel history. Different investigators have addressed and discussed the basic assumptions used in the TopModel. Questions about the distribution of soil hydraulic conductivity, number of parameters and the hypothesis of hydrological similarity of saturated areas (hypothesis 1) have been investigated and modifications have been proposed (e.g., parabolic, non-exponential transmissivity profiles, etc).

An example of this type of investigation is exemplified by Lane et al. (2004) in which the connectivity of water parcel trajectories between areas of similar topographic index is considered. On the other hand, the version called Dynamic TopModel (Metcalfe, Beven & Freer 2015) also considers the issue of similarity, proposing to replace it with the kinematic wave solution, as a way

to replace hypothesis 1, which is obtained at the expense of an increase in the number of model parameters and of introduction of complexity of more robust numerical formulations (higher order positively defined advection) to eliminate numerical instabilities from the solution of the hyperbolic wave equation (in finite differences or finite elements) (Beven, Kirkby & Freer 2021).

Another aspect of the TopModel was the preparation of the global mapping of the topographic index (*topidx*) in high resolution (15 arc seconds) by Marthews et al. (2015). The field of this surface index associated with the unique definition of water parcel trajectories over the terrain is the essential boundary condition of the TopModel. The proposition by Marthews et al. (2015) aims to use the TopModel for all river basins on the planet, however if on the one hand it provides the essential parameter of the model, on the other hand it highlights that the model was developed for small basins, provided that the hypothesis of rain and infiltration homogeneous in space and variable in time is used for the derivation of TopModel equations that imply conditions of hydrological similarity.

Karam, Pereira Filho and Flores Rojas (2017) proposed an approach applying the variational principle to this question, relaxing the need for spatial homogeneity of the atmospheric precipitation field (and also of infiltration), by using a variational functional under weak constraint, associated with mass conservation over time and minimum length paths for the water plots. Thus, modifications of the original topographic index are obtained as a function of both the local derivative of precipitation and its movement, in an Eulerian frame of reference.

In the present work, the R code corresponding to the original version of Beven and Kirkby (1979) in Fortran-77 is used, as available in R (R-TopModel library), prepared and distributed by Buytaert (2022). In the simulation ahead, the topographic index is a two-dimensional invariant.

The topographic index obtained with R-TopModel is used to map the boundary conditions of the landslide and flood hazard models (i.e., the soil saturation deficit and the surface water excess, respectively).

2.6 GLUE Method to Parameters Tuning

The GLUE optimization method is a brute-force method that explores values in defined ranges of variations for each TopModel parameter, thus obtaining combinations among the possible random choices of parameter values.

Each combination of parameters is used to obtain a simulation member whose efficiency is evaluated. Generated members that produce simulation with higher efficiencies are separated and organized according to the obtained Nash-Sutcliffe efficiency, resulting in an ensemble.

In general, the parameter set (best ensemble) can be composed of 100 members or more, so a quantile distribution analysis can be readily obtained. The quantile analysis once performed results in the median output and confidence interval of the members of the ensemble along the time coordinates. Quantiles of 5% and 95% are commonly presented in the results (e.g., Beven, Kirkby & Freer 2021) that is followed here.

2.7 ANOVA and Homoscedasticity

An analysis of variance (one-way ANOVA) with verification of homoscedasticity was applied to verify the general validity of the hypothesis of normality of the covariance of errors used in linear structure models, following Chambers, Freeny and Heiberger (2017). Specifically, one-way ANOVA was applied to test the significance of the result obtained with a linear regression model, used as an approximation of non-linear models such as TopModel.

A non-linear model may differ from surface water wave conservation solutions such as the one obtained for a kinematic wave implemented in the dynamic TopModel. In the original TopModel (available in R-TopModel) convergence-divergence can occur along the surface water path (implicitly since no wave equation is explicitly solved).

As the input structure (precipitation and potential evapotranspiration data) and output structure of the original TopModel (river flow) presents likelihood (which is evident from the literature), the model can basically be ideally represented and simplified by a convolution of the function input by one or more Gaussian functions that serve as a time-phased filter.

In general, the ANOVA analysis is valid if the results (modelistic and observational) can be considered as drawn from the same set, differing from the expected values of the statistical model by values within a small statistical tolerance (e.g., 5%).

In summary, the verification of homoscedasticity was carried out considering the TopModel as a generalization of a linear structure model. One-way ANOVA was used to verify the necessary similarity between the model input and output error structures. The implementation of TopModel in R follows Bevans (2022).

2.8 Landslide Hazard Model and Flood Risk Assessment

The R-TopModel distribution model has been used to estimate both the height of excess water above the surface (i.e., defined by the precipitation rate minus the infiltration rate multiplied by the time step) and the distribution of water

in the topsoil layer (1 – Saturation Deficit). The associated dangerousness depends on the amplitude of these variables, while the risk depends on the dangerousness, exposure and vulnerability of the population. The spatial distribution of dangerousness can be overlap with the population map that varies throughout the day in risk areas. In general, the vulnerability also varies associated with health, age and mobility. In this way a contingent risk results.

2.8.1. Landslide Hazard Model

Tatizana et al. (1987a, 1987b) developed empirical curves that are useful for landslide risk analysis (single and multiple) based on the adjoint analysis of the hourly precipitation rate and the accumulated over the period of 24, 48, 72 and 96 hours. These curves are currently used in emergency management centers in Brazil. In the methodology proposed in this work, the approach is based on physics, that is, the effect of rain and humidity on soil cohesion, compression and shear stresses, friction force between soil layers on the slope, layer safety factor soil surface and its failure probability.

The stability is a function of the equilibrium condition between two opposite forces: first, the disruptive tangential force, and second, the friction force that resists the disruption and relative movement of layers.

The wetting of the soil by precipitation causes both an increase in the density of the soil, with the consequent increase both in the weight of the layer and the shear stress of the inclined terrain, as also this leads to decrease in cohesion, with associated decreasing of the friction force. For a dry soil, the weight by volume unity (γ_d) in units of (N m^{-3}) is presented by Equation 1,

$$\gamma_d = (g\rho_d) \tag{1}$$

For humid soil column between surface and the water table below the soil wetness, and the associated saturation water deficit is limited to the interval [0;1], $A_g \in [0;1]$ and $D_g \in [0;1]$ while $\alpha \in [0;[$ and $D \in];1]$.

The excess of water over the soil surface can be expressed through Equation 2,

$$\alpha_{excess} = (\alpha - 1) \tag{2}$$

This occurs always $\alpha > 1$ or $D < 0$ associated with an excess of rainwater accumulated above the soil surface. The soil density variation when the soil is moistened ($\Delta\rho$) (kg m^{-3}) is defined by Equation 3,

$$\Delta\rho = (\eta\alpha_g \rho_w) \tag{3}$$

The wet soil density is described in Equation 4,

$$\rho_g = \rho_d + \Delta\rho \tag{4}$$

For humid soils, we have to consider effects associated with the soil upper layer volumetric fraction of water or soil upper layer wetness (α_g) and the corresponding soil upper layer water saturation deficit (D_g), both with values limited to the interval [0;1].

The excess of water over the surface is obtained always the total water available (α) is larger than soil capacity, this is represented by Equation 5,

$$\alpha_{excess} = (\alpha - 1) > 1 \tag{5}$$

The wet soil density [ρ_g] (kg m^{-3}) considers the replenishing of water by soil pores, given by the Equation 6,

$$\alpha_{vol} = \eta\alpha_g \tag{6}$$

Note that α_{vol} is obtained from the product of porosity (η) and soil upper layer wetness (α_g). The soil weight by volume unity in unit of (N m^{-3}) is expressed by Equation 7,

$$\gamma_c = g\rho_g \tag{7}$$

An estimation of the effective friction coefficient is parameterized by Equation 8,

$$tan(\varphi_{eff}) = \varphi_{max} exp(-\alpha_g) \tag{8}$$

In the function of the soil wetness. The dry soil cohesion is obtained using Equation 9,

$$C_d = (\gamma_d z_w) \tag{9}$$

The humid soil cohesion (in Pa) is given by Equation 10,

$$C = \gamma z_w \tag{10}$$

The cohesion variation due to moistening of the upper soil layer by rainfall is expressed by Equation 11,

$$\Delta C = C - C_d \tag{11}$$

The normal stress tensor component (in Pa) is given by Equation 12,

$$\sigma = \gamma z_w cos^2(\theta)/c_z \tag{12}$$

where the denominator is obtained using 13,

$$c_z = exp(-\alpha_g) exp(-sin\theta) \tag{13}$$

The tangent stress tensor component, in (Pa), is expressed in Equation 14,

$$\tau = (\gamma_c z_w)\,[sin(\theta)cos(\theta)]/c_w \quad (14)$$

The resistance force (N) in accord with De Blasio (2011) is formulated by Equation 15,

$$F_R = (\Delta x \Delta y)\,[\sigma\, tan(\varphi) + C\,] \quad (15)$$

The water height above the surface (m) is estimated by Equation 16,

$$H_{excess} = (z_w \eta \alpha_g) + (r\Delta t) \quad (16)$$

The external pressure (C_e) considers only two natural factors: i) the weight force due to the accumulated water depth above the surface; ii) the weight force due to the water excess on the surface from the actual precipitation (r), given by Equation 17,

$$C_e = (g\rho_w)(h_{scar}\eta\alpha_{excess} + r\Delta t) \quad (17)$$

The safety factor (F) is expressed by Equation 18,

$$F = 0.9 + \alpha_0\,(\alpha_1\alpha_2\alpha_3\alpha_4) \quad (18)$$

where the hazard factors of F are represented by Equation 19,

$$\begin{aligned} \alpha_0 &= exp[-(tan\theta - tan\varphi)/\,tan\,\varphi], \\ \alpha_1 &= exp(-\Delta\rho_s/\rho_{sd}), \\ \alpha_2 &= exp(-\alpha_g), \\ \alpha_3 &= exp(-\Delta C/C_d), \\ \alpha_4 &= exp(-\Delta C_e/C_d). \end{aligned} \quad (19)$$

where $\Delta\rho_s$ and ρ_{sd} are the wet soil density increment and dry soil density; α_g is the volumetric fraction of soil water; ΔC is the wet soil cohesion absolute reduction of the soil cohesion, and ΔC_e is the external pressure variation associated with the water in excess over the surface and dynamic pressure due to the impact of drops during rainfall, directly associated is the saturation deficit variation up to rupture, given by Equation 20,

$$\Delta D = F - 0.90 \quad (20)$$

With these estimations, the critical rainfall (r_c) to be provided up to the upper soil layer rupture can be expressed by Equation 21,

$$r_c = r_{scale}\,[exp(\Delta D\text{-}1)]^{1.125} \quad (21)$$

where r_{scale} is the prior value of rainfall associated with landslide hazard, locally or regionally defined (here, 30 mm h^{-1}). Finally, the probability of landslides, $Prob\{\mu\}$ is the following accumulated probability logistic function as shown in Equation 22,

$$Prob\{\mu\} = 1 - 1/(1+e^{\mu}) \quad (22)$$

where the hazard metrics μ *is* given by the Equation 23,

$$\mu = (r - r_c)/\sigma_m \quad (23)$$

r is the actual rainfall, and σ_m is the margin of discriminant risk curve (supposed equal to 25% of r_{scale}). $Prob\{\mu\}$ is the probability cumulative distribution function (CDF), obtained by integration of the associated function density of probability between 0 and μ. A landslide hazard mask is used as a binary indicator function, with value 1 is used to indicate a surface element with landslide hazard probability larger than 50% and value 0, otherwise. The total number of landslides by time step in the simulated area is evaluated using two comparative proxies: the data-based proxy, expressed through Equation 24,

$$n_{lsd}(1) = r\,R_{24h}/(3200 mm^2 h^{-1}) - 1 \quad (24)$$

with r (in mm h^{-1}) and R_{24h} (in mm), with r R_{24h} greater than 3200, and the modeled proxy, represented by Equation 25,

$$n_{lsd}(2) = 24\%[Prob(\mu) - 0.5] \quad (25)$$

The parameters used in the present landslide hazard model are given in Table 1.

2.8.2. Flood risk Assessment

An one-dimensional Gaussian filter convolution is applied to the topography field in the directions x and y resulting in a convoluted topography (z_{conv}). The original topographic field is subtracted from the convoluted one to obtain the 2D distribution of the height to be overcome. This height needs to be surpassed whenever the river overflows. The Gaussian filter convolution is equivalent to a more complex Han's convolution for circular boundary frontiers with FFT, but without the need for periodic lateral boundaries.

The local surface water height threshold for overflow $\Delta z_{bank}(x,y)$ is obtained by Equation 26,

$$\Delta z_{bank}(x,y) = z_{conv}(x,y) - z(x,y) - min\{z_{conv}\} + min\{z\} \quad (26)$$

The excess water on the local surface (i.e., the part of precipitation not infiltrated) is standardized as shown in Equation 27.

$$\mu(x,y) = [Water_{Excess}(x,y) - \Delta z_{bank}(x,y)]/\Delta z_{bank}(x,y) \quad (27)$$

Table 1 Parameters of the landslide hazard model. Range references: (1) Coelho Netto (1996); (2) Deardorff (1978); (3) Sellers (1960); (5) De Blasio (2011); (6) D'Orsi, Feijo and Paes (2002, 2004) and D'Orsi (2016), (*) this work.

Par.	Meaning	Values(*)	Usual Range	Unit	Ref.
r_{scale}	Landslide hazard critical rainfall	30	30 – 60	(mm h^{-1})	(6)
σ_m	Rainfall margin of the discriminant curve	4	10 – 60	(mm h^{-1})	(6),(*)
z_w	Mean water table depth	4	0.25 – 25	(m)	(2)
ρ_{sd}	Mean dry soil density	1600	900 – 2500	(kg m^{-3})	(3)
$tan\ \varphi$	Mean friction coefficient	1	0.01 – ∞	(-)	(5)
η	Mean soil porosity	0.40	0.01 – 0.45	(-)	(3)

The distribution of the flood hazard probability ($Prob_F$) (%) is then represented by a logistic model, as shown in Equation 28,

$$Prob_F = 1 - 1/[1 + exp(\mu)] \quad (28)$$

A categorical distribution can be associated with the dimensional values to support immediate decision actions. A associated categorical flood risk assessment for every river station can be defined by the ratio between the river deep (D) and the maximum height of the river bank max{D}, being this later depends on the position of the rated station along the stream. A useful categorical set proposition for qualifying flood risk is given by: monitoring (watching): D/D_{max}<50%, warning: 50%≤D/D_{max}<80%, alert: 80%≤D/D_{max}<90%, high alert: 80%≤ D/D_{max}<90%, and overflow (plain flood): 100%≤ D/D_{max}, which one associated with specific actions by emergency managers. For instance, similar thresholds are currently in use by the Institute of the Environment of the State of Rio de Janeiro in Brazil (Inea-RJ 2023), based in location rated monitoring river stations for short-term nowcasting to risk prone areas.

2.8.3. Numerical Verifications

In a new model approach, as presented in this work, has considered some scale relation model to checking built methods. For instance, the stream flow scales could be checked by comparison to the station rated scale model of Williams (1978). In this case, the flow scale relations are given by Equation 29,

$$\begin{aligned} Q_m &= V, \\ Q_b &= W, \\ Q_f &= D. \end{aligned} \quad (29)$$

where Q is the stream flow in ($m^3\ s^{-1}$), V is the mean stream velocity, W is the mean stream width W (m) and D is the stream deep (m). For consistency, the sum of the exponents (m, b, and f) equals one. As Q is provided at each time step by a water-routing model, flow scales can be readily estimated in a first approximation and utilized for verifications.

3 Results

The digital terrain topography of Carsington Water watershed, measurements of rainfall and stream outflow were prepared to used in the hydrological model. The topography of England from the digital elevation model is shown in Figure 1. The spatial resolution is 16 km^2 enough to show mountain peaks with an altitude of up to 1000 m (amsl). This coarse resolution digital elevation model (DEM) was prepared to further use in a proxy risk assessment online.

Carsington Water dam is located in east-central England. A local radar high resolution digital elevation model was used to obtain the topography in the interest area of Carsington Water watershed (Figure 2).

One alternative to obtain 2D rainfall fields every hour is the Hydroestimator/NOAA (Scofield 1987; Scofield & Kuligowski 2003; Vicente, Scofield & Menzel 1998). Alternatively, in this work is used daily rainfall data series composed by 365 days, as have been provided by UK Weather Office, attending the application for the small catchment (i.e., 15.8 km^2 Carsington Water catchment area).

Considered a benchmark, the Lake Carsington Water watershed was chosen (latitude: +53.061438717°N, longitude: -1.6282852790°W), located between the cities of Birmingham and Sheffield, south of the national park Pick District National Park in Matlock-UK.

Time series reanalysis of measured water volume outflow at Carsington station observed in border of the Lake Carsington Water were used for comparison with the modeled results and calibration using GLUE method. A series of parameters and corresponding solutions present adequate likelihood. Values of parameters in combinations with the other parameters showing higher NS efficiencies

were separated to generate a set of members of ensemble solutions.

The final result of the flow modeling after GLUE calibration and assembly member generation is that the vast majority of observed values are within the confidence interval defined by the evolution of the 5 and 95% quantiles of the ensemble members. Good model performance was obtained by generation of ensemble members resulting NS > 30%. A number of the best members are selected to the final quantile analysis. General agreement between simulation and observation was found but presenting some dispersion into linear regression fit. The confidence interval of 5 and 95% were presented in Figure 4. The maximum NS was near to 65%, enough high considering the method limitations and simplifications (e.g., TopModel hypothesis of forcing homogeneity, defined soil water transmissibility profile, steady solution, unity hydrograph and first-order similarity).

The distribution of members of the ensemble allows the presentation of the thresholds of the Probability allows a link with the reality of the observed flow, since it allows decision-making in the face of the costs of preventive measures and the value of losses associated with not taking preparatory measures. The deviations from the modeled and observed flow are shown in Figure 4. Most of the values of 100% can be seen considering the concentration of a surface catchment area. These deviations can be associated with the concentration time scale and river celerity. Typical values are up to 1.2 m s^{-1}. In general, rivers contained in the primary channel present celerities between 0.1 and 1.2 m s^{-1}. Simulation bias shows variations over the simulation period. By excluding the initial spin-up period of the model, the bias value can be limited [-1.5; +1.5], probably associated with excess runoff.

The quantile-quantile diagrams were obtained for the linear regressions and for TopModel flow. Generally, the TopModel performs reasonably well (NSE>60%) in the range of mean flows, with a confidence interval between Q5% and Q95%. However, underestimates are expected for extreme flows.

3.1 Test of Homoscedasticity and Uncertainties of Linear Regression

To assess the validity of the TopModel nonlinearity hypothesis a test of homoscedasticity and uncertainties of linear regression was realized, as a linear approach of the more general validity conditions is required for modeling. Homoscedasticity was verified by one- and two-way ANOVA, represented by Qobs ~ Rain and Qobs ~ Rain+ETp, respectively. Thus, it was possible to verify large deviations of the linear regression in relation to the diagonal in relation to the expected quantile (Normal), mainly for lower and higher values. In this work, homoscedasticity was not confirmed beyond the central range of flow values. The non-normality of the precipitation is already known in the literature. Therefore, it confirms that rainfall-runoff modeling by nonlinear physics-based models or by generalized statistical regression models is recommended.

Filtered precipitation time series were generated to evaluate the relative importance of the different time scales present in the original series. A post-hoc F-test of non-additivity for two-way ANOVA (Tukey 1949, 1962) revealed that the higher frequency scales of the data are not present in part of the observed flow data during the summer. A wavelet analysis (not shown) confirmed the absence of these higher frequency signals in the river discharge value, while suggesting the important role of potential evapotranspiration from the dam in the summer months. Thus, Tukey's post-hoc test of filtered series results in a greater association with the low frequencies of the annual cycle.

In fact, a subsequent group comparison (Akaike information criterion, AIC) also resulted in greater flow gains in the linear composition of precipitation and potential evapotranspiration throughout the year, especially in the British Isles summer (values not shown). The annual variation of potential evapotranspiration is important for describing the water surface balance. The composition of the linear regression of the filtered data series indicates the main role of seasonal changes in precipitation and evapotranspiration, suggesting that these compositions are more advantageous for stream-flow modeling in the parametric conditions of the hydrological model, that is, when potential evapotranspiration decreases atmospheric forcing.

The statistical summary of the variables is shown in Table 2. Although the observed and simulated discharge present comparable averages, the same does not happen for the corresponding medians. The inter-quartile is close but the extremes are different. Therefore, the TopModel modeling presents limitation outside the inter-quartile interval.

The ANOVA brought the stream flow problem to light. Since the Carsington soil surface is highly permeable to infiltration and evapotranspiration, can contributes effectively to the aquifers westward on Midland of England.

Table 3 summarizes results from one-way ANOVA, and Tables 4 from two-way ANOVA. It is evident that the main predictor role of atmospheric forcing (i.e., precipitation minus potential evapotranspiration) for the Carsington Water dam overflow, for annual period. Tables 4 and 5 summarize the interaction between predictor and

Table 2 Summary of variable statistics (Qobs, Qsim, rain, ETp).

X	Qobs ($m^3 s^{-1}$)	Qsim ($m^3 s^{-1}$)	rain ($m s^{-1}$)	ETp ($m s^{-1}$)
Min.	0.01000	0.006467	3.615×10^{-11}	0.000×10^{00}
1st Qu.	0.02314	0.020174	7.261×10^{-09}	8.653×10^{-09}
Median	0.36552	0.069307	2.252×10^{-08}	2.893×10^{-08}
Mean	1.12001	1.114237	2.793×10^{-08}	2.906×10^{-08}
3rd Qu.	1.69823	1.890884	4.449×10^{-08}	4.964×10^{-08}
Max.	9.01115	6.156999	1.163×10^{-07}	5.810×10^{-08}

predicted variables and presents the degree of statistical significance of the iterations, with greater F associated with greater statistical confidence.

The hydrological model should account for the larger expected changes in space and time. At this point, TopModel has the advantage of being an efficient distributing model. The creek flow freely emerging from Carsington Water dam could be modeled by TopModel in function of the topographic index, parameters, rainfall and potential evapotranspiration data series (Figure 4).

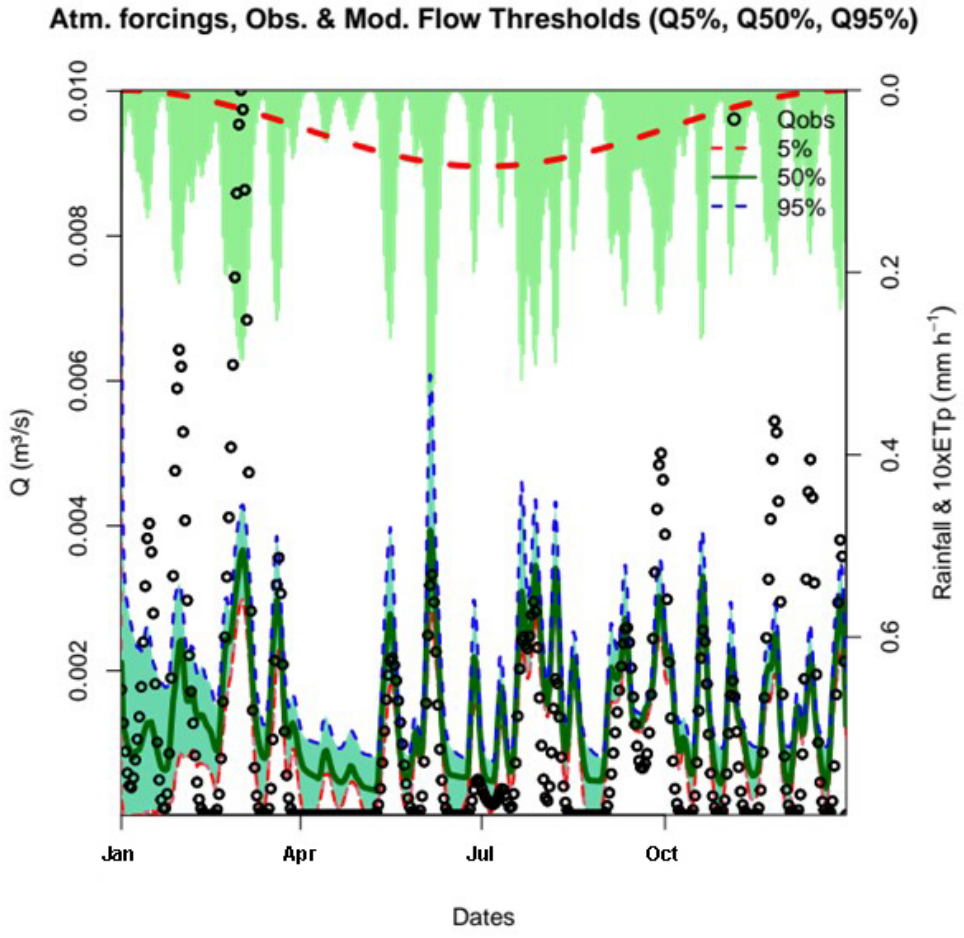

Figure 4 Comparison of the flow modeled by TopModel and observed at the monitoring point of the stream emerging from the Carsington Water dam, throughout 2017. The flow due to surface runoff (i.e., the observed flow minus the basic flow) is represented by open circles, precipitation by impulse in light green, potential evapotranspiration by the thick dashed line highlighted in red, the confidence interval by the area filled in green estimated by modeled quantiles between 5% and 90%, and the simulated flow median indicated by the dark green line.

The model performance improves its performance with GLUE parameters generation. GRUE generation provides different ensemble members, each one associated with Nash-Sutcliffe efficiency larger than 50%. The associated stream flows are ranked to obtain quantiles curves. The ensemble median is given by the 50% quantile, and the confidence interval limited by the quantiles of 5% and 95%.

3.2 Hydrometeorological Hazards Assessment

The coupling of the hydrological model, giving the distribution of water in the surface layer of the soil, with the models of landslides on slopes and of floods due to the overflow of riverbeds, allows access to risk from the point of view of conditional probability. This realization generates the contingent probability (median Q50% of the danger).

Figure 5 shows the 2D distribution of landslide (Figures 5A and 5B) and flood hazard (Figures 5C and 5D).

The greater danger of landslides is confirmed in the hills to the north and west of the Carsington Water dam, as well as the greater danger of water overflowing from the creeks as the drainage network progressively increases its drainage of the land (to the south and east of the dam).

By adding observation errors of atmospheric forcing by a Normal distribution generating function, it is even possible to extend the analysis to an ensemble of model tests. An analysis of the distribution of members (i.e., 2D fields) allows inferring the variability of the median and its statistical confidence thresholds.

Table 3 Summary of one-way ANOVAS.

Var	Df	Sum Sq	Mean Sq	F value	Pr(>F)	Signif.
Summary of one-way ANOVA (Qobs ~ rain)						
rain	1	463.7	463.7	373.2	$< 2 \times 10^{-16}$	***
Residuals		363	450.9	1.2		
Summary of one-way ANOVA (Qobs ~ Etp)						
Etp	1	70.0	70.01	30.09	7.75×10^{-08}	***
Residuals		363	844.6	2.33		

Signif. Codes: 0 '***' 0.001 '**' 0.01 '*' 0.05 '.' 0.1 ' '

Table 4 Summary of two-way ANOVA (Qobs ~ rain + Etp).

Var	Df	Sum Sq	Mean Sq	F value	Pr(>F)	Signif.
rain	1	463.7	463.7	453.06	$< 2 \times 10^{-16}$	***
Etp	1	80.5	80.5	78.62	$< 2 \times 10^{-16}$	***
Residuals		362	370.5	1.0		

Signif. Codes: 0 '***' 0.001 '**' 0.01 '*' 0.05 '.' 0.1 ' '

Table 5 Summary of ANOVA interations (Qobs ~ Qobs * rain * ETp).

Var	Df	Sum Sq	Mean Sq	F value	Pr(>F)	Signif.
rain	1	463.7	463.7	4235.06	$< 2 \times 10^{-16}$	***
Etp	1	80.5	80.5	734.94	$< 2 \times 10^{-16}$	***
Qobs:rain	1	298.3	298.3	2725.01	$< 2 \times 10^{-16}$	***
Qobs:Etp	1	0.0	0.0	0.35	0.554	
rain:Etp	1	14.6	14.6	133.00	$< 2 \times 10^{-16}$	***
Qobs:rain:Etp	1	18.3	18.3	167.51	$< 2 \times 10^{-16}$	***
Residuals	358	39.2	0.1			

Signif. Codes: 0 '***' 0.001 '**' 0.01 '*' 0.05 '.' 0.1 ' '

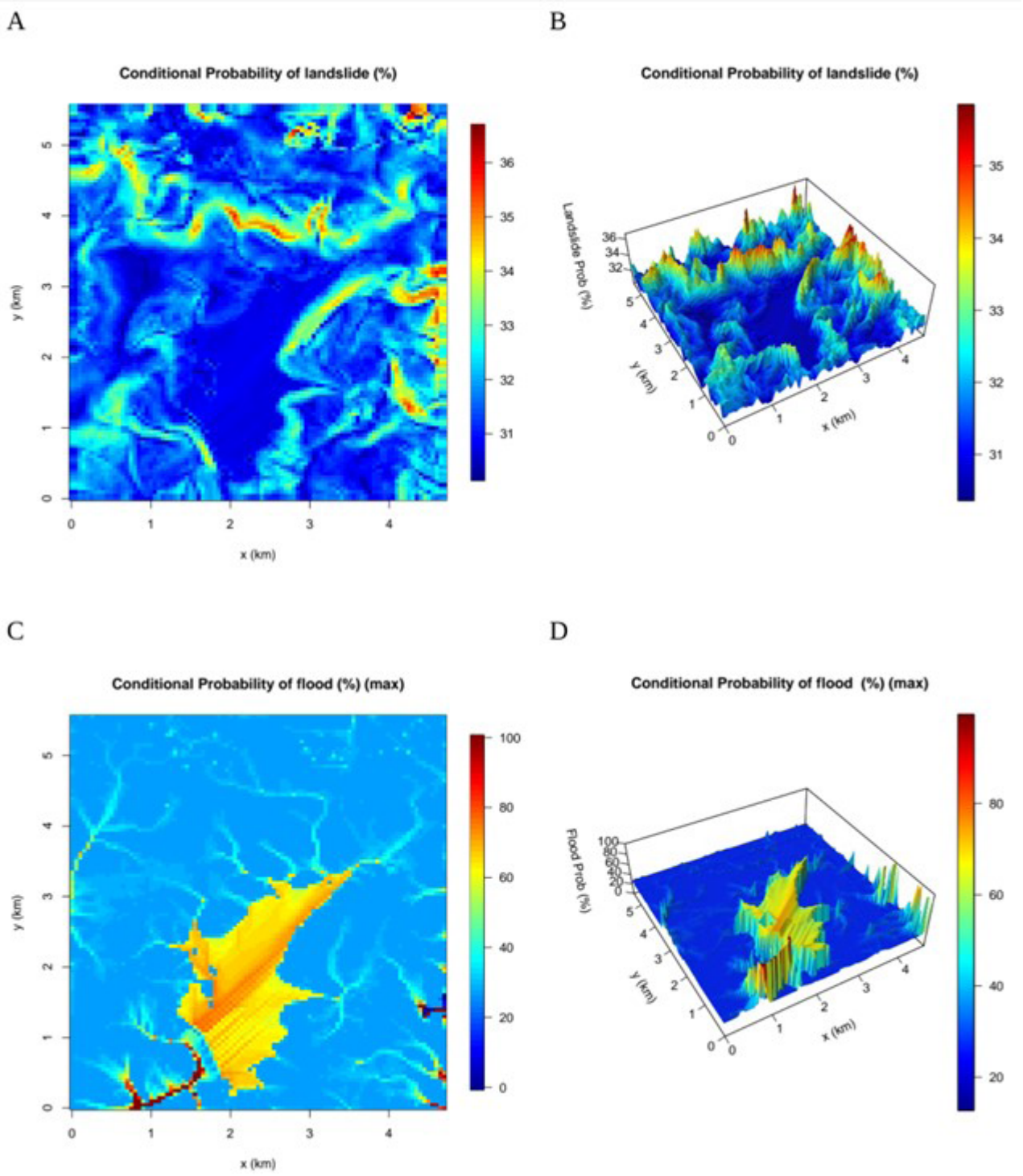

Figure 5 Modeled distribution of maximum hydrometeorological hazard probability in 2017 for the Carsington Dam catchment, in Midland of England: **A.** Conditional landslide hazard probability (%); **B.** Perspective view of A; **C.** Conditional flood hazard Probability (%); **D.** Perspective view of C. These spatial distributions correspond to the day of maximum atmospheric forcing in the data series of 2017.

The area corresponding to landslide and flood hazards is sensitive to the magnitude of the atmospheric forcing (verified numerically), making it possible to generate different scenarios according to the intensity of the precipitation rate. This can be important for land planning and governance (e.g., decision-making about higher-risk areas that should be designated for preservation).

3.3 Verification of Model Results

The timescale of atmospheric precipitation systems, as well as the intrinsic characteristics of the watershed, are important for river response. For multi-scale systems, validations with multi-category prediction methods seem to be recommended (WWRP/WGNE 2017, Wilks 2019). Here, a verification of flooding results was carried out qualitatively by comparing the modeled risk areas with low frequency occurrence maps (UK Flooding Maps 2023).

Flood management centers generally focus on measuring the height of rivers and assessing overflow conditions. Forecast models for very short periods of areas at risk of flooding, in general, need to assess the probability of immediate risk in addition to the values of the increase in water height, to allow decision-making from a few minutes to a day before the event. In a dynamic approach, rapidly updating flood hazard maps can be superimposed on population maps and integrated by geographic information systems in automatic updated.

Similarly, a qualitative evaluation of the results of the landslide distribution model was made from comparison with maps of historical landslide records in the area (National Landslide Database 2023).

4 Conclusions

Digital terrain model and time series of precipitation, evapotranspiration and discharge measured at the outlet of the Carsington Water dam were used as input data in an original coupled system formed by the hydrological model (R-TopModel) and skilled landslide and flood risk models. The results are positive and indicate the possibility of operational use of the methodology, to map the distribution of hydrometeorological risks at each time step. In this work, the time step was daily, but it can be done in higher temporal resolution if hourly monitoring is available.

Some statistical analyzes of the input data, for example one-way and two-way ANOVA, time-scale filtering and wavelet analysis confirm the importance of atmospheric forcings (precipitation and evapotranspiration) for a qualified flow simulation in the Carsington Water flow. The results were obtained and evaluated to serve as a benchmark for further investigations (e.g., as such the development of an online dynamic hazard model for landslides and flooding in comparable basins of tropical and mid-latitude size).

In perspective, Beven and Wood (1983) and Lane et al. (2004) made relevant contributions to the modeling of wetlands under complicated conditions of topographic variation and high spatial resolution. To do so, the former applied variable contribution areas associated with approximation of the slope geometry (linear or curved) and the latter applied drainage network indices to direct the flow paths to obtain different degrees of connectivity at grid points, resulting in minimal areas connected by saturation.

In addition to the temporal variability of the forcings and the topological connectivity of the water path, the application of the Variational Principle to the conservation of mass along the water paths makes it possible to determine the trajectory in a unique way, considering the effect of the spatial heterogeneities of the atmospheric forcings as strong constraints of the problem.

Looking further, the use of satellite-derived precipitation would allow applying the methodology for analysis of short-term events in different areas simultaneously, which would be important for the verification and validation process of the complex hydrological system for known risk areas from historical database of landslides and floods.

5 Acknowledgments

To the CONFAP/British Council cooperation program that enabled the second author to travel to Brazil (Process FAPERJ no. E-26/203104/2019).

6 References

Bevans, R. 2022, *ANOVA in R – A Complete Step-by-Step Guide with Examples,* Scribbr, viewed 26 May 2023, <https://www.scribbr.com/statistics/anova-in-r>.

Beven, K. & Wood, E.F. 1983, 'Catchment geomorphology and the dynamics of runoff contributing areas', *Journal of Hydrology*, vol. 65, no. 1-3, pp. 139-58, DOI:10.1016/0022-1694(83)90214-7.

Beven, K.J. & Kirkby, M.J. 1979, 'A physically based, variable contributing area model of basin hydrology', *Hydrological Sciences Bulletin*, vol. 24, no. 1, pp. 43-69, DOI:10.1080/02626667909491834.

Beven, K.J., M.J. Kirkby, J.E. & Freer, R.L. 2021, 'A history of TopModel', *Hydrology and Earth System Sciences*, vol. 25, no. 2, pp. 527-49, DOI:10.5194/hess-25-527-2021.

Burt, S. 2010, 'British rainfall 1860–1993', Weather, vol. 65, no. 5, pp. 121-8, DOI:10.1002/wea.603.

Buytaert, W. 2022, *TopModel: Implementation of the Hydrological Model TopModel*, R. Library R-TopModel, viewed 26 May 2023, <https://github.com/ICHydro/TopModel/>.

Chambers, J.M., Freeny, A. & Heiberger, R.M. 2017, 'Analysis of variance; designed experiments', in S.J.M. Chambers & T.J. Hastie (eds), *Statistical models*, Wadsworth & Brooks/ Cole, Pacific Grove, pp. 145-93.

Coelho Netto, A.L. 1996, 'Produção de Sedimentos em Bacias Fluviais Florestadas do Maciço da Tijuca, RJ: respostas aos eventos extremos de fevereiro de 1996', paper presented at Proceedings of II Encontro Nacional de Engenharia de Sedimentos, vol. 1, pp. 209-17.

D'Orsi, R.N., Feijo, L. & Paes, N.M. 2002, *Relatório de escorregamentos*, Fundação Geo-Rio Report, Rio de Janeiro.

Danielson, J.J. & Gesch, D.B. 2011, Global multi-resolution terrain elevation data 2010 (GMTED2010), U.S. Geological Survey Open-File Report 2011–1073, 34 p, viewed 26 May 2023, <https://pubs.usgs.gov/of/2011/1073/pdf/of2011-1073.pdf>.

De Blasio, F.V. 2011, *Introduction to the physics of landslides: Lecture notes on the dynamics of mass wasting*, Springer Science & Business Media.

Deardorff, J.W. 1978, 'Efficient prediction of ground surface temperature and moisture, with the inclusion of a layer of vegetation', *Journal of Geophysical Research: Oceans*, vol. 83, no. C4, pp. 1889-903, DOI:10.1029/JC083iC04p01889.

Devia, G.K., Ganasri, B.P. & Dwarakish, G.S. 2015, 'A review on hydrological models', *Aquatic Procedia*, vol. 4, pp. 1001-7, DOI:10.1016/j.aqpro.2015.02.126.

D'Orsi, R.N. 2016, *Lecture about GeoRio Fundation*, AlertaRio System of the Municipality of Rio de Janeiro-RJ, Brazil, 85 slides.

D'Orsi, R.N., Feijo, R.L. & Paes, N.M. 2004, '2,500 operational days of Alerta Rio system: History and technical improvements of Rio de Janeiro warning system for severe weather', in W. Lacerda, M. Ehrlich, S.A.B. Fontoura & A.S.F. Sayao (eds), *Landslides: Evaluation and stabilization*, Taylor & Francis Group, London, pp. 831-6.

ED-UK 2023, *Henmore Brook Catch (trib of R Dove)*, Departament for Environment Food & Rural Affairs-UK, viewed 26 May 2023, <https://environment.data.gov.uk/catchment-planning/WaterBody/GB104028052700>.

Environment Agency-UK 2023, *Flood warnings, river levels and flood risk maps*, UK, viewed 26 May 2023, <https://www.gov.uk/government/organisations/environment-agency>.

Froude, M.J. & Petley, D.N. 2018, 'Global fatal landslide occurrence from 2004 to 2016', *Natural Hazards and Earth System Sciences*, vol. 18, no. 8, pp. 2161-81, DOI:10.5194/nhess-18-2161-2018.

Gomez, H. & Kavzoglu, T. 2005, 'Assessment of shallow landslide susceptibility using artificial neural networks in Jabonosa River Basin, Venezuela', *Engineering Geology*, vol. 78, no. 1-2, pp. 11-27, DOI:10.1016/j.enggeo.2004.10.004.

INEA-RJ – Instituto Estadual do Ambiente 2023, *State Institute of the Environment of the State of Rio de Janeiro*, Brazil.

Karam, H.A. 2014, 'Modelagem da distribuição da saturação de água do solo em terrenos complexos baseada na teoria de similaridade – proposição de abordagem lagrangiana', *Anuário do Instituto de Geociências*, vol. 37, no. 2, pp. 139-50, DOI:10.11137/2014_2_139_150.

Karam, H.A., Pereira Filho, A.J. & Flores Rojas, J.L. 2017, 'On the precipitation homogeneity hypothesis in the TopModel applications', *Revista Brasileira de Cartografia*, vol. 69, no. 1, pp. 13-22, DOI:10.14393/rbcv69n1-44028.

Keller, V.D.J., Tanguy, M., Prosdocimi, I., Terry, J.A., Hitt, O., Cole, S.J., Fry, M., Morris, D.G. & Dixon, H. 2015, 'CEH-GEAR: 1 km resolution daily and monthly areal rainfall estimates for the UK for hydrological and other applications', *Earth System Science Data*, vol. 7, no. 1, pp. 143-55, DOI:10.5194/essd-7-143-2015.

Lane, S.N., Brookes, C.J., Kirkby, A.J. & Holden, J. 2004, 'A network-index-based version of TopModel for use with high-resolution digital topographic data', *Hydrological Processes*, vol. 18, no. 1, pp. 191-201, DOI:10.1002/hyp.5208.

Marsh, T.J. & Hannaford, J. (eds) 2008, *UK hydrometric register*, Centre for Ecology & Hydrology.

Marthews, T.R., Dadson, S.J., Lehner, B., Abele, S. & Gedney, N. 2015, 'High-resolution global topographic index values for use in large-scale hydrological modelling', *Hydrology Earth System Sciences*, vol. 19, no. 1, pp. 91-104, DOI:10.5194/hess-19-91-2015.

Metcalfe, P., Beven, K. & Freer, J. 2015, 'Dynamic TOPMODEL: A new implementation in R and its sensitivity to time and space steps', *Environmental Modelling & Software*, vol. 72, pp. 155-72, DOI:10.1016/j.envsoft.2015.06.010.

National Landslide Database 2023, *British Geological Survey*, BGS Research, United Kingdom, viewed 26 May 2023, <https://www.bgs.ac.uk/datasets/national-landslide-database/>.

Ordnance Survey 2017, *OS TERRAIN 50 User guide and technical specification* v1.3, UK digital topography source, Crown Publ., 33 p., viewed 26 May 2023, <https://www.ordnancesurvey.co.uk/documents/os-terrain-50-user-guide.pdf>.

Peña, A.C.S. 2018, 'Desenvolvimento de um modelo numérico para a avaliação de riscos naturais associados à precipitação na RMRJ', Master thesis, Universidade Federal do Rio de Janeiro, Rio de Janeiro.

Preti, F. & Letterio, T. 2015, 'Shallow landslide susceptibility assessment in a data-poor region of Guatemala (Comitancillo municipality)', *Journal of Agricultural Engineering*, vol. 46, no. 3, pp. 85-94, DOI:10.4081/jae.2015.450.

Scofield, R.A. & Kuligowski, R.J. 2003, 'Status and outlook of operational satellite precipitation algorithms for extreme-precipitation events', *Monthly Weather Review*, vol. 18, pp. 1037-51, DOI:10.1175/1520-0434(2003)018<1037:SAOOOS>2.0.CO;2.

Scofield, R.A. 1987, 'The NESDIS operational convective precipitation estimation technique', *Monthly Weather Review*, vol. 115, pp. 1773-92, DOI:10.1175/1520-0493(1987)115<1773:tnocpe>2.0.co;2.

Sellers, W.D. 1960, *Physical climatology*, University of Chicago Press, Chicago.

Siqueira, B.S. 2017, 'Investigação do papel da precipitação para análise de risco de deslizamentos de encostas', Master thesis, Universidade Federal do Rio de Janeiro, Rio de Janeiro.

Tatizana, C., Ogura, A.T., Cerri, L.E.S. & Rocha, M.C.M. 1987a, 'Análise da correlação entre chuvas e escorregamentos na

Serra do Mar, município de Cubatão', paper presented at Proceedings of the 5th Congresso Brasileiro de Geologia de Engenharia, São Paulo, vol. 2, pp. 225-36.

Tatizana, C., Ogura, A.T., Cerri, L.E.S. & Rocha, M.C.M. 1987b, 'Modelamento numérico da análise de correlação entre chuvas e escorregamentos aplicado às encostas da Serra do Mar no município de Cubatão', paper presented at Proceedings of Congresso Brasileiro de Geologia de Engenharia (5th), São Paulo, vol. 2, pp. 237-48.

Tukey, J.W. 1949, 'One degree freedom for non-additivity', *Biometrics*, vol. 5, no. 3, pp. 232-42, DOI:10.2307/3001938.

Tukey, J.W. 1962, 'The Future of Data Analysis', *The Annals of Mathematical Statistics, Institute of Mathematical Statistics Stable*, vol. 33, no. 1, pp. 1-67.

UK Flooding Maps 2023, *Check the long term flood risk for an area in England*, Environment and Countryside Flooding and Extreme Weather (UK post area: Water Rail Carsington Water Ashbourne DE6 1ST), viewed 26 May 2023, <https://check-long-term-flood-risk.service.gov.uk/search>.

Vicente, G.A., Scofield, R.A. & Menzel W.P. 1998, 'The operational GOES infrared rainfall estimation technique', *Bulletin of the American Meteorological Society*, vol. 79, no. 9, pp. 1883-98.

Wilks, D. 2019, *Statistical methods in the atmospheric sciences*, 4th edn, Elsevier.

Williams, G.P. 1978, *Hydraulic geometry of river cross-sections: Theory of minimum variance*, vol. 1029, Department of the Interior, Geological Survey, Washington, D.C.

WWRP/WGNE 2017, 'Forecast verification methods across time and space scales of the joint working group on forecast verification research', paper presented at 7th International Verification Methods Workshop, Berlin, Germany.

Author contributions

Hugo Abi Karam: project; conceptualization; formal analysis; methodology; numerical implementation; verification-validation; writing-original draft; writing – review and editing; visualization; discussions. **Matthew Alexander Blackett:** project; conceptualization; formal analysis; methodology; validation; discussions. **Raphaella Barros Pereira da Silva**, **Jose Luis Flores Rojas** and **Augusto José Pereira Filho**: formal conceptual analysis; numerical discussions; verifications. **Cesar Arturo Sanchez Peña, Isela Leonor Vásquez Panduro, Brenda Santos Siqueira** and **Julio Miguel Angeles Suazo:** conceptual discussions.

Conflict of interest

The authors declare no conflict of interest.

Data availability statement

Reference datasets, scripts and code are available on request.

Funding information

The CONFAP/British Council cooperation program facilitated the visit of the second author to Brazil for a brief period (FAPERJ Process No. E-26/203104/2019).

Editor-in-chief

Dr. Claudine Dereczynski

Associate Editor

Dr. Gerson Cardoso da Silva Jr.

How to cite:

Karam, H.A., Blackett, M.A., Silva, R.B.P., Flores Rojas, J.L., Pereira Filho, A.J., Sanchez P., C.A., Vásquez P., I.L., Siqueira, B.S. & Suazo, J.M.A. 2024, 'Modeling of Soil Water Distribution in a Small Mid-Latitude Watershed on the British Isle for Short Term Landslide and Flood Risk Assessment', *Anuário do Instituto de Geociências,* 47:57297. https://doi.org/10.11137/1982-3908_2024_47_57297